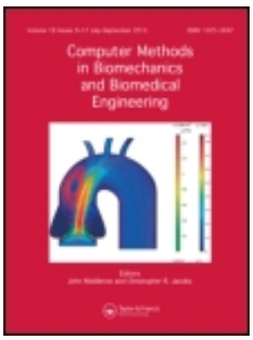

Taylor & Francis
Taylor & Francis Group

Computer Methods in Biomechanics and Biomedical Engineering

ISSN: 1025-5842 (Print) 1476-8259 (Online) Journal homepage: http://www.tandfonline.com/loi/gcmb20

The effects of knee joint kinematics on anterior cruciate ligament injury and articular cartilage damage

Alexander D. Orsi, Srinath Chakravarthy, Paul K. Canavan, Estefanía Peña, Ruben Goebel, Askhan Vaziri & Hamid Nayeb-Hashemi

To cite this article: Alexander D. Orsi, Srinath Chakravarthy, Paul K. Canavan, Estefanía Peña, Ruben Goebel, Askhan Vaziri & Hamid Nayeb-Hashemi (2016) The effects of knee joint kinematics on anterior cruciate ligament injury and articular cartilage damage, Computer Methods in Biomechanics and Biomedical Engineering, 19:5, 493-506, DOI: 10.1080/10255842.2015.1043626

To link to this article: http://dx.doi.org/10.1080/10255842.2015.1043626

Computer Methods in Biomechanics and Biomedical Engineering, 2016
Vol. 19, No. 5, 493–506, http://dx.doi.org/10.1080/10255842.2015.1043626

The effects of knee joint kinematics on anterior cruciate ligament injury and articular cartilage damage

Alexander D. Orsi[a], Srinath Chakravarthy[a], Paul K. Canavan[b], Estefanía Peña[c], Ruben Goebel[d], Askhan Vaziri[a] and Hamid Nayeb-Hashemi[a]*

[a]*Biomechanics Research Group, 334 Snell Engineering Center, Northeastern University, 360 Huntington Avenue, Boston, MA, USA;* [b]*Hartford HealthCare Rehabilitation Network, 230 Main St, Manchester, CT, USA;* [c]*Bioengineering Division, Aragon Institute of Engineering Research, University of Zaragoza, CIBER de Bioingeniería, Biomateriales y Nanomedicina (CIBER-BBN), Zaragoza, Spain;* [d]*Sport Science Program, Qatar University, Doha, Qatar*

(*Received 24 October 2014; accepted 19 April 2015*)

This study determined which knee joint motions lead to anterior cruciate ligament (ACL) rupture with the knee at 25° of flexion. The knee was subjected to internal and external rotations, as well as varus and valgus motions. A failure locus representing the relationship between these motions and ACL rupture was established using finite element simulations. This study also considered possible concomitant injuries to the tibial articular cartilage prior to ACL injury. The posterolateral bundle of the ACL demonstrated higher rupture susceptibility than the anteromedial bundle. The average varus angular displacement required for ACL failure was 46.6% lower compared to the average valgus angular displacement. Femoral external rotation decreased the frontal plane angle required for ACL failure by 27.5% compared to internal rotation. Tibial articular cartilage damage initiated prior to ACL failure in all valgus simulations. The results from this investigation agreed well with other experimental and analytical investigations. This study provides a greater understanding of the various knee joint motion combinations leading to ACL injury and articular cartilage damage.

Keywords: anterior cruciate ligament; failure locus; finite element; injury

1. Introduction

The anterior cruciate ligament (ACL) is a major stabilizing ligament of the knee. The ACL is known to prevent anterior tibial displacement relative to the femur, and provide torsional stability during internal and external rotations (Girgis et al. 1975; Markolf et al. 1976; Butler et al. 1980; Grood et al. 1981; Fukubayashi et al. 1982). The ACL originates anterior and medial to the tibial eminence, rising posteriorly and laterally, inserting on the lateral wall of the femoral intercondylar notch (Girgis et al. 1975; Arnoczky 1983; Amis and Dawkins 1991; Takahashi et al. 2006). ACL tears are painful injuries, and are reported to occur from 250,000 to 400,000 times annually in the United States. (Boden, Dean, et al. 2000; Boden, Griffin, et al. 2000; Griffin et al. 2006; Fleming et al. 2010; Smith et al. 2012; Nau and Teuschl 2015). Reconstructive surgery and rehabilitation are expensive procedures which put significant burden on the healthcare system (Feagin and Lambert 1985; Boden, Dean, et al. 2000; Boden, Griffin, et al. 2000; Griffin et al. 2006). It is known that articular cartilage and meniscal injuries are commonly associated alongside ACL injury. These combined ACL/articular cartilage injuries are also known as major risk factors for degenerative osteoarthritis later in life (Vellet et al. 1991; Johnson et al. 1998; Faber et al. 1999). It is clinically important to determine which movement combinations are likely to cause injury to knee joint tissues, as an improved understanding of these injury mechanisms will improve prevention techniques, rehabilitation, and surgical procedures (Renstrom et al. 2008).

ACL injuries are classified by two mechanisms: contact and non-contact. ACL injuries commonly occur in non-contact scenarios (McNair et al. 1990). Several studies report non-contact ACL injury occurring with athletes landing near full knee extension, in valgus, and in femoral external rotation (McNair et al. 1990; Ferretti et al. 1992; Malone et al. 1993; Ireland 1999; Boden, Dean, et al. 2000; Boden, Griffin, et al. 2000; Griffin et al. 2006). These studies also described a deceleration closed chain mechanism associated with ACL injury. The knee was reported to be within 20°–30° of knee flexion at injury (McNair et al. 1990; Ireland 1999; Boden, Dean, et al. 2000; Boden, Griffin, et al. 2000; Besier et al. 2001). Video evidence has reported the main contributors to non-contact ACL injuries are motions in the frontal and transverse planes (Boden, Dean, et al. 2000; Boden, Griffin, et al. 2000; Olsen et al. 2004; Krosshaug et al. 2007).

While cadaver testing is the gold standard for studying the mechanics of soft tissue, computational models are

*Corresponding author. Email: hamid@coe.neu.edu

improving, and are being used more widely due to the limitations of cadaver testing. Investigating ligament and soft tissue failure for various knee joint motions using cadaveric knees would be cost and time prohibitive. A single cadaver sample provides only one failure result as the original state cannot be restored after the ACL is torn. Because of this, a number of cadavers would be required to establish an injury locus. Furthermore, developing a failure locus using multiple cadaver samples would not be advantageous as each sample would have individual geometries, creating sample-to-sample variations in the results. In contrast, finite element (FE) models can simulate multiple failures using different loading scenarios for an individual knee joint model. Computational models also provide a method to investigate subject specificity as it is known that every subject has unique bone and soft tissue geometries (Bisson and Gurske-DePerio 2010; Hashemi et al. 2010; Simon et al. 2010). Using this method, a subject specific set of failure data points, known as a failure locus, can be generated. The present study used a 3D FE model to perform a parametric analysis of knee joint motions to generate a failure locus. The failure locus included bundle specific failure data for the ACL along with articular cartilage injury data. The failure locus is based on Varus/Valgus (V/V) angle and Internal/External (I/E) rotation when the knee is at 25° of flexion. Knee flexion at 25° was chosen as this is within the range of flexion angles commonly observed during ACL injury (McNair et al. 1990; Ireland 1999; Boden, Dean, et al. 2000; Boden, Griffin, et al. 2000; Besier et al. 2001). Axial stress within the ACL, and shear stress within the articular cartilage were monitored during FE simulations, allowing for virtual injury diagnoses.

Previous studies have used 3D FE knee joint models to investigate the stress and strain fields in knee joint tissues under various loading conditions (Gardiner and Weiss 2003; Limbert 2004; Mesfar and Shirazi-Adl 2006; Peña et al. 2006; Papaioannou et al. 2008, 2010; Boyd et al. 2012; Wangerin 2013; Kiapour et al. 2014; Wang et al. 2014). Soft tissue injury was not investigated in any of these studies. Peña et al. (2006) investigated the effect of combined loading on the stress field in the ligaments and menisci. In the study, Peña et al. (2006) validated that subject specific FE knee joint models can accurately predict the stresses and strains seen in these tissues under complex loading. Mesfar and Shirazi-Adl (2006) investigated the effects of changes in pretension and material properties in the cruciate ligaments on the biomechanics of the knee joint. The results of their study highlighted that incorrectly applied ligament prestrain can significantly affect the natural motion of the knee joint (Mesfar and Shirazi-Adl 2006). Limbert (2004) modeled the ACL as a single bundle with and without prestrain and investigated the differences in ligament stress during passive flexion. The results of their study closely resembled results from cadaver testing in terms of the resultant force in the ligament during passive knee flexion (Limbert 2004). Limbert (2004) assumed uniform prestretch throughout the ACL, which the authors stated as a limitation. Gardiner and Weiss (2003) performed a subject specific study on eight sample cadaver knees to study the stress–strain behavior of the medial collateral ligament (MCL) during knee joint loading. Each knee underwent valgus loading at different knee flexion angles during which kinematic and strain data was collected. Material properties were obtained through uniaxial testing of the eight MCL specimens. FE models of the bony geometries and the MCL were constructed from volumetric CT image data for each subject. The unique MCL material properties extracted from the uniaxial testing of each specimen were applied to each FE model. Each model was validated by comparing the experimental results to the FE predictions of MCL strain during valgus loading. Gardiner and Weiss (2003) demonstrated that the complex non-uniform *in vivo* strain fields seen in the MCL under valgus loading can be accurately predicted using FE techniques. Kiapour et al. (2014) developed a 3D FE model of a knee subjected to different loading conditions. They demonstrated their FE models accurately predict soft tissue stresses and joint kinematics. Kiapour et al. (2014) state that their model will be used to determine risk factors for ACL injury in the future. These studies have all produced useful results by modeling the knee joint using FE analysis to monitor the stresses and strains in tissues under specific loading schemes. There were no studies found using FE knee models to investigate the effect of various knee joint motions on ACL injury and concomitant injuries.

The purpose of the present study was to determine which knee joint motions are most detrimental to the ACL and articular cartilage at 25° of knee flexion. By displaying the relative dangers between the designated knee motions, the failure locus identifies knee motions that should be avoided. This study produces useful information for improving orthopaedic care by better understanding how these injuries occur. The results will help healthcare professionals improve injury prevention programs.

2. Methods

In order to develop a reliable model and to validate our results based on available experimental data and available numerical investigations, we considered the following important details.

(1) Time dependent material properties were not used in this model. Preliminary FE simulations performed at physiologically accurate loading rates using a time dependent material model revealed no significant variation in the frontal plane knee angle at ACL failure, compared to

corresponding time independent simulations (Orsi 2015). Hence, a transversely isotropic hyperelastic model was chosen for the ACL in this study. This model accurately represents the response of cadaveric ACL, and is more computationally efficient compared to the rate dependent material.

(2) It is known that a variable axis of rotation has been proposed for the knee flexion axis (Hollister et al. 1993). Research has validated the transepicondylar axis as an optimal axis for representing proper knee flexion (Churchill et al. 1998). Also, the transepicondylar axis was used in several previous investigations, and the results were in good agreement with experimental data (Yang et al. 2010a; Homyk et al. 2012). For these reasons, in this investigation the knee flexion axis of rotation was chosen to be the transepicondylar axis.

(3) Displacement driven analyses were used instead of force driven analyses for several reasons. Accounting for muscle force contribution in a force driven analysis is very inaccurate. Muscle forces are not constant, and to record these muscle forces experimentally for the motions of interest would be inaccurate. Displacement controlled FE analyses provide a way to bypass these limitations. This is useful as the displacement based injury results can be compared to video evidence which is also displacement based. If an accurate model can be established which accounts for the contributions of the musculature and other soft tissues during stress analyses of the knee joint, the stress field would correspond to the same kinematics used in the present investigation (compatibility condition). A number of investigators have used force driven analyses to understand the stresses within the knee joint soft tissues (Haut Donahue et al. 2003; Peña et al. 2006; Kiapour et al. 2014). Studies have also used displacement driven analyses to study the knee joint soft tissue stresses (Gardiner and Weiss 2003; Song et al. 2004; Park et al. 2010). The boundary conditions for these displacement controlled simulations are generally extracted from cadaver experiments. As the present study simulates several different failure modes for the ACL, obtaining experimental cadaver data for this would be extremely difficult, as each cadaver knee is capable of only one ACL failure.

A subject-specific 3D FE model of a left knee was created from sagittal view magnetic resonance images (MRI) of a healthy 26-year-old male with a frontal plane alignment angle of 7.67° valgus, seen in Figure 1 using the method provided by Homyk et al. (2012) and Yang et al. (2010a), similar to Haut Donahue et al. (2003).[1] Images were obtained using short bore, high-field 1.5 Tesla MRI and a fat suppressed fast spin echo sequence with a TE = 10 ms, 160 × 160 mm field of view, and slice thickness of 2 mm with 256 × 256 matrix. A similar model was successfully used in our previous investigation (Yang et al. 2009; Yang et al. 2010a, 2010b; Homyk et al. 2012[2]). The subject was imaged early in the morning and had been unloaded for 30 minutes prior to imaging to minimize a full day of weight bearing. This was done to preserve the native geometry of the cartilage and menisci, as the geometries of these tissues have been reported to change due to body weight loading (Herberhold et al. 1999; Vedi et al. 1999; Gründer et al. 2000; Nishii et al. 2008). This may have prevented erroneous measurement of the ACL length at full knee extension, which is required in our subsequent analyses. However, we believe that the error in ACL length measured from MRI after a full day of load bearing would be small. The MRIs of the subject were taken in the supine, non-load-bearing position. They were converted into 3D solid structures using Rhinoceros and SolidWorks; these solid structures were then imported into ABAQUS and converted to an FE mesh.

A free meshing technique was used for the cartilage and meniscus using four-node linear tetrahedral elements. The ACL was meshed using hexahedral elements. The model included a total of 40,793 nodes with 160,522 elements. The cartilage mesh size was between 0.8 and 1.0 mm, while the meniscus mesh size was 0.5 mm, and the ACL was meshed at an average size of 1.0 mm. A mesh sensitivity analysis was performed and an optimum mesh size was selected based on less than a 5% difference from the subsequently higher mesh density. For example, under body weight loading there was only a 2.76% difference in peak cartilage stress between the chosen mesh size (density = 0.8 mm) and the next higher mesh size (density = 0.6 mm). Linear elements, in conjunction with material incompressibility, may lead to volumetric locking resulting in higher stresses (Askes et al. 1999). This problem can be overcome by using higher order elements, using refined mesh, or reduced integration. Also, the reduced integration scheme may result in an erroneous solution, or no solution at all (Bell et al. 1993). For these reasons, both refined linear and quadratic elements were used. Both approaches produced the same results, and fine tetrahedron elements were adopted for the cartilage and meniscus in all simulations. This substantially reduced computational time.

Bone was modeled as rigid, as it is much stiffer than the soft tissue it interacts with (Fung and Zhang 2003; Haut Donahue et al. 2003; Yang et al. 2010a; Homyk et al. 2012). The articular cartilage was modeled as isotropic linear elastic and the meniscus was modeled as transversely isotropic linear elastic, with the material properties shown in Table 1. Linear elastic material properties were appropriate in this study as similar

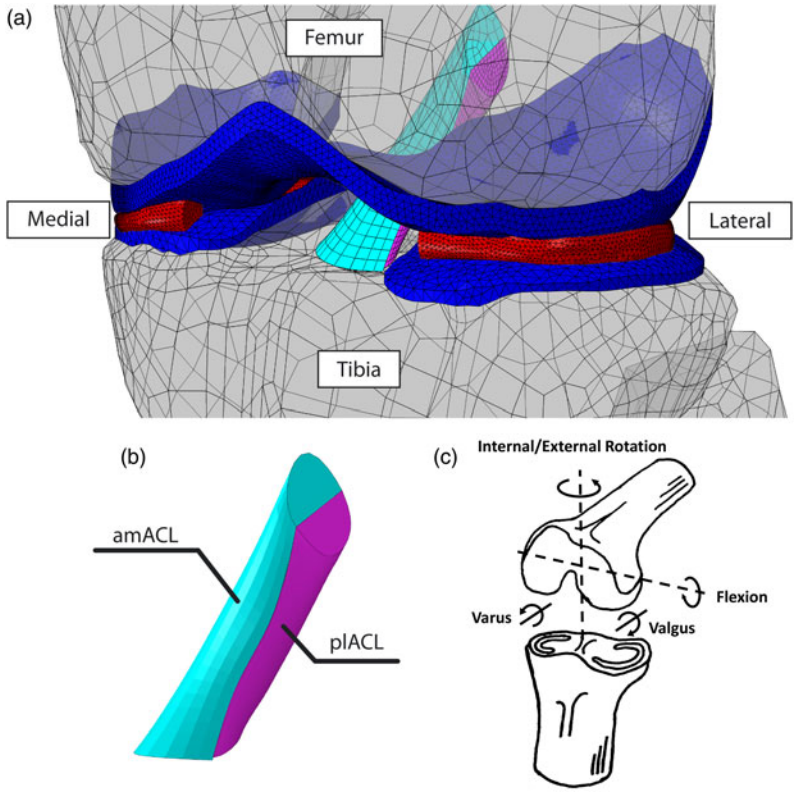

Figure 1. (a) Anterior view: 3D FE model of left knee joint. Bone is shown as transparent, meshed with four node bilinear rigid quadratic elements. Articular cartilage is shown in dark blue and meniscus is shown in red, both were meshed using linear tetrahedron elements. The ACL bundles are detailed in (b), the amACL shown in light blue and the plACL shown in purple, both meshed with eight node brick elements. (c) Boundary condition reference for the failure locus simulations performed.

techniques have been used to model cartilage and meniscus in several previous studies (Haut Donohue et al. 2002; Haut Donahue et al. 2003; Yang et al. 2010a; Wangerin 2013; Kiapour et al. 2014). The menisci were attached to the tibial plateau at the meniscal horns using linear spring element sets, similar to the methods used by Haut Donahue et al. (2003) and Yang et al. (2010a). At each horn attachment 10 linear springs were used to attach the meniscal horn to the tibial plateau. A transverse ligament was modeled as a single spring element, which attached the anterior horns of the menisci to each other (Haut Donahue et al. 2003; Yang et al. 2010a; Homyk et al. 2012).

There were six contact interactions between the femoral articular cartilage, the tibial articular cartilage and the medial and lateral menisci. All contact was modeled using a frictionless finite-sliding formulation where separation and sliding of finite amplitude and arbitrary rotation of the surfaces are allowed. Contact interaction normal to the contacting surfaces was constrained using the standard penalty enforcement method.

The posterior cruciate ligament (PCL), MCL, and lateral collateral ligament (LCL) were modeled as multi bundled nonlinear spring elements. 3D structures were considered for these ligaments, specifically to see if interaction existed between the ACL and PCL. The results indicated no interaction between the ACL and PCL existed for the range of motion used in this study (Orsi 2015). This validated modeling the PCL, MCL, and LCL as spring

Table 1. Cartilage and meniscus material properties.

Tissue	Constitutive model	Properties
Cartilage	Isotropic elastic	$E = 15.0$ MPa, $v = 0.45$
Meniscus	Transversely isotropic elastic	$E_\theta = 140$ MPa, $E_r = E_z = 20$ MPa $v_{rz} = 0.2, v_{r\theta} = v_{z\theta} = 0.3$ $G_{r\theta} = G_{z\theta} = 57.7$ MPa, $G_{rz} = 8.33$ MPa

Source: Homyk et al. (2012), Kiapour et al. (2014), Haut Donahue et al. (2003) and Yang et al. (2010a).

elements, while providing an accurate estimation of the stresses in the ACL, and substantially reducing computational intensity. Ligament insertion sites were determined from the MRI, similar to the group's previous work (Yang et al. 2010a; Homyk et al. 2012). The nonlinear spring force-displacement relationship used is defined as a piecewise continuous function,

$$f = \begin{cases} \frac{(1/4)k\epsilon^2}{\epsilon_l}, & 0 \le \epsilon \le 2\epsilon_l \\ k(\epsilon - \epsilon_l), & \epsilon > 2\epsilon_l \\ 0, & \epsilon < 0, \end{cases} \quad (1)$$

where f is the tensile force, k is a stiffness parameter, and $2\epsilon_l$ is the lower bound strain limit for the linear ligament behavior. ϵ is the strain in the ligaments defined as $\epsilon = (L - L_0)/L_0$, where L is the ligament length and L_0 is the unstretched zero-load length of the ligament. At full knee extension the initial reference strain, ϵ_r, is listed in Table 2 for each bundle. L_0 is found using ϵ_r along with the initial reference length of the ligament, L_r, using $L_0 = L_r/(\epsilon_r + 1)$, where L_r is determined from the MRI as the distance between the tibial and femoral insertion sites. This study modeled the PCL as a double bundle (anterior and posterior bundle). The LCL and MCL were modeled with three bundles. The properties of each ligament were adapted from the work of Blankevoort et al. (1991), shown in Table 2 (Blankevoort et al. 1991).

2.1 ACL modeling

Studies report the ACL as comprising two main bundles, the anteromedial bundle (amACL) and posterolateral bundle (plACL) (Girgis et al. 1975; Blankevoort et al. 1991; Sinkov et al. 2004; Peña et al. 2006; Takahashi et al. 2006; Steckel et al. 2007). This composition was chosen for modeling the ACL in this study. In full knee extension, both bundles are parallel and under prestrain. The prestrain values are provided by Blankevoort et al. (1991) and are listed in Table 3, showing the plACL has a higher prestrain at full extension than the amACL. During larger degrees of knee flexion the amACL increases in tension and the plACL decreases in tension (Blankevoort et al. 1991). The 3D structure of the double bundle ACL is shown in Figure 1(b). The bundle cross sections and insertion sites were determined from the MRI, and were validated based on anatomical studies (Girgis et al. 1975; Takahashi et al. 2006). The bundles were created by lofting from both insertion sites to mid-substance uniform cross section regions using SolidWorks 2010 (DassaultSystemes, Concord, MA, USA). This produced ligament structures at the reference length, L_r, seen in Figure 2(a). $L_r$was defined as the distance between the centroids of the insertion sites. The ligament bundles were then resized from L_r to L_0, based on the data provided by Blankevoort et al. (1991) in Table 3. This was done by transecting the bundles in their uniform regions according to their prestrain values. The transected bundles were then reattached to achieve zero-load length structures, shown in Figure 2. The superior (red) portions remained fixed to the femur, while the inferior (blue) portions were translated superiorly to attach to the superior (red) portions. This created zero-load length structures able to develop prestrain during extension from L_0 to L_r during FE simulation. The 3D structures were then meshed using ABAQUS (Simulia, Providence, RI, USA).

Table 2. Material properties for nonlinear spring ligaments (PCL, LCL, MCL).

Ligament	Bundle	Stiffness parameter, k[N]	ϵ_r
PCL	Anterior	9000	−0.24
	Posterior	9000	−0.03
LCL	Anterior	2000	−0.25
	Superior	2000	−0.05
	Posterior	2000	0.08
MCL	Anterior	2750	0.04
	Inferior	2750	0.04
	Posterior	2750	0.03

Source: Adopted from Blankevoort et al. (1991).

Table 3. Initial prestrain data for ACL bundles.

ACL bundle	% Prestrain	L_r (mm)	L_0 (mm)
plACL	10.0	24.54	22.08
amACL	6.0	27.57	25.91

Using a user subroutine, a fiber orientation dependent transversely isotropic hyperelastic material, defined by a strain energy density, ψ was used to obtain the constitutive equations of the ACL (Puso et al. 1998). The strain energy density was defined as,

$$\psi = C_1(\tilde{I}_1 - 3) + C_2(\tilde{I}_2 - 3) + F_2(\tilde{\lambda}) + \frac{K}{2}(\ln(J))^2, \quad (2)$$

where J is the Jacobian of the deformation gradient F defined as $\partial x/\partial X$ where x and X are coordinates of each point in the deformed and undeformed configurations. C_1 and C_2 are constants representing the Mooney-Rivlin material model and K is the bulk modulus of the material. $\tilde{I}_1$ and $\tilde{I}_2$ are the first and second invariant of the modified Cauchy-Green strain tensor $\bar{\mathbf{C}} = J^{-2/3}\mathbf{F}^T\mathbf{F}$. The derivative of the fiber strain energy function F_2 defined in Equation (3) (Puso et al. 1998) is given as,

$$\tilde{\lambda}\frac{\partial F_2}{\partial \tilde{\lambda}} = \begin{cases} 0, & \tilde{\lambda} \le 1 \\ C_3\left[e^{C_4(\tilde{\lambda}-1)} - 1\right], & 1 < \tilde{\lambda} < \lambda^* \\ C_5\tilde{\lambda} + C_6, & \tilde{\lambda} \ge \lambda^* \end{cases} \quad (3)$$

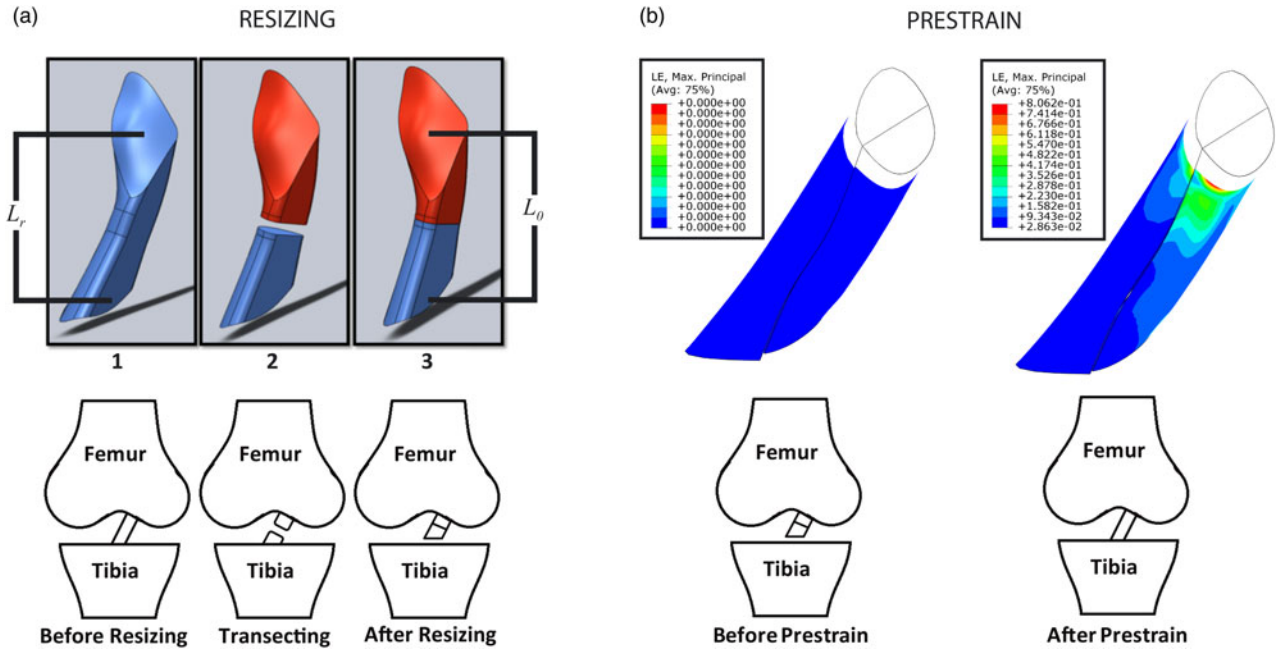

Figure 2. (a) Outline of ACL resizing process. The bundles were initially created at the reference length (L_r). They were then transected in the midsubstance according to their prestrain values. The bundles were then reconnected to create an unstretched structure at the zero load length (L_0). (b) ACL prestrain simulation showing the ligament stretching from L_0 to L_r, creating the bundle specific strain which is present at full knee extension. LE is defined as maximum principal strain.

The first relationship reflects the inability of ligament structures to support compressive loads. The second relationship is the nonlinear 'toe region' corresponding to the uncrimping of the collagen fibers. The third corresponds to the linear stress-stretch response of the straightened fibers. λ^* is the amount of stretch at which the material transitions from unstraightened to straightened fibers. $\tilde{\lambda}$ is defined as the deviatoric stretch along the fiber direction. The material constants were extracted from the work of Peña et al. (2006). These constants are shown in Table 4. Fiber direction was defined by the lines between the tibial and femoral insertion sites for both ligament bundles.

As stated earlier, to simulate *in vivo* prestrain of the ACL at full knee extension, the ACL bundles were stretched from their zero-load lengths to their reference lengths. Figure 2 shows the double bundle ACL structure undergoing the simulated *in vivo* prestrain inherent in the ACL at full knee extension.

2.2 *Spring ligament validation*

While ligaments are 3D structures, modeling them as spring structures reduces complexity whereas there is no interaction between ligaments and bony surfaces. As the purpose of this research was to investigate which combinations of knee joint movements (displacements) create mid substance rupture within the ACL bundles, it was necessary to investigate if there was interaction between the ligaments of interest within the range of motions considered in this investigation. To determine if this was a factor, a preliminary study investigated PCL–ACL interaction for the knee motions considered, and determined whether the spring model was appropriate for modeling the PCL in order to reduce computation cost. The 3D PCL was constructed from MRI, similar to the ACL construction method described in the previous section. Four extreme case knee motions were simulated to monitor PCL–ACL interactions. Each simulation started with the ACL prestrained followed by 25° knee flexion. The four simulations investigated were; (i) 15° internal femoral rotation (IR) with varus angle applied until ACL failure, (ii) 15° IR with valgus angle applied until ACL failure, (iii) 15° external femoral rotation (ER) with varus angle applied until ACL failure, and (iv) 15° ER with valgus angle applied until ACL failure. The ACL failure results from these simulations were compared to those obtained from the PCL spring ligament model. No significant differences were found regarding the stress distribution in the ACL or the failure angles, and no contact between the ACL and PCL was observed, justifying the use of nonlinear springs in modeling the PCL for the range of motions considered in this investigation.

Table 4. Material coefficients for the ACL.

C_1 (MPa)	C_2	C_3 (MPa)	C_4	C_5 (MPa)	λ^*	K
1.95	0.0	0.0139	116.22	535.039	1.046	1950

2.3 Failure criterion

Previous investigations have reported on the ultimate tensile strength of the ACL using cadaveric knees. Woo et al. (1991) determined the ultimate failure load for ACL from nine separate young donors to be 2160 ± 157 N. Kennedy et al. (1976) determined the ultimate failure load to be 625 ± 22 N. Noyes et al. (1976) determined the ultimate failure load for the ACL to be 1730 ± 660 N. The failure load determined by Woo et al. (1991) was adapted for this study as Kennedy et al. (1976) had a high median age for the donors (62 years), and Noyes et al. (1976) used a smaller sample size of six samples from three young donors. The lower bound from Woo et al. (1991) was selected corresponding to a failure force of 2003 N. To adapt this for a 3D structure, the axial force was converted to an axial true stress using $\sigma_t = (F/A_0)(1+\epsilon)$. F is the failure force, A_0 is the cross sectional area of the ACL bundles, ϵ is the engineering strain at failure determined from Blankevoort et al. (1991), and σ_t is the corresponding true failure stress. Both bundles had identical mid-substance cross sectional areas, ($A_0 = 23.04\,\text{mm}^2$). The axial failure force was divided between the bundles and the true failure stress at tear initiation was determined to be 50.2 MPa. Butler et al. (1986) found the average failure stress for the ACL to be 36.4 MPa. This value was found using the engineering stress at ACL failure from a small sample size of three subjects. Using true stress would greatly change this result which could explain the difference between the failure stress used in this investigation and the failure stress reported by Butler et al. (1986).

The articular cartilage failure criterion for this study was adapted from the work of Atkinson et al. (1998). They determined that articular cartilage fissuring is caused primarily from shear stress initiated at the surface of the articular cartilage. The authors suggested a critical shear stress of 4.15 MPa is required to initiate articular cartilage fissuring. In this study, when the maximum shear stress in the articular cartilage reached 4.15 MPa, cartilage was assumed to have been damaged. The critical shear stress obtained by Atkinson et al. (1998) should be considered as the lower bound shear stress required to initiate cartilage damage. It is known that fluid pressure in the cartilage may result in higher critical shear stress for damage initiation. As there is no available critical shear stress for cartilage damage obtained through *in vivo* experiments, we used 4.15 MPa as the critical shear stress damage criterion. This limitation may apply to all available mechanical properties obtained through *in vitro* experiments.

As the simulations are under displacement control, the kinematics needed for ACL failure will not be affected by the initiation of cartilage fissuring. The extent of articular cartilage damage reported at ACL injury may be inaccurate due to changes in the material properties of damaged cartilage. Currently there is no accurate data regarding the constitutive equations for damaged cartilage. The extent of cartilage damage reported at ACL injury should be considered an underestimation as a damage model was not used. As stated earlier the knee joint motions required for ACL injury were not affected by cartilage injury in these simulations as the simulations were under displacement control. This further demonstrates that displacement control should be considered as a proper method for investigating many injuries in future research.

2.4 Sequential loading validation

Two simulations were performed to validate that loading sequence had no significant effect on the results. In the first validation simulation knee flexion was applied initially, followed by simultaneous IR and valgus loading until ACL failure. IR angles were recorded at ACL failure from this simulation for use in the second validation simulation. In the second validation simulation, knee flexion and IR were applied simultaneously, followed by valgus loading until failure. There was negligible difference in the valgus angle at ACL failure between the first and second validation simulations, indicating that ACL failure is independent of loading sequence in these simulations.

2.5 Failure locus simulations

Fourteen simulations were conducted with knee flexion held at 25°, as this angle is reported to be within the range of maximum injury susceptibility (Ireland 1999; Boden, Dean, et al. 2000; Boden, Griffin, et al. 2000; Besier et al. 2001). Each simulation was a five step quasi-static sequential loading analysis with the following order; (i) ligament prestrain, (ii) 3.6 × body weight, (iii) knee flexion, (iv) axial femoral rotation, and (v) valgus or varus angular displacement. As this model does not consider muscle forces, the body weight was adjusted to 3.6 × body weight to account for joint compression due to muscle contraction. This value was used to simulate the maximum compressive joint force during gait and was applied through the midpoint of the trans-epicondylar axis, consistent with previous investigations (Yang et al. 2010a). Furthermore, we believe body weight does not contribute significantly to ACL failure in this investigation. Excessive body weight may slightly reduce the ACL pretension, however the main contributors to ACL stresses are I/E rotation and V/V motion. 25° knee flexion was applied through the trans-epicondylar axis of the femur as this axis has been determined as the optimum knee flexion axis (Churchill et al. 1998). In this investigation, the relative motion between the femur and tibia is important. One can move the femur with respect to

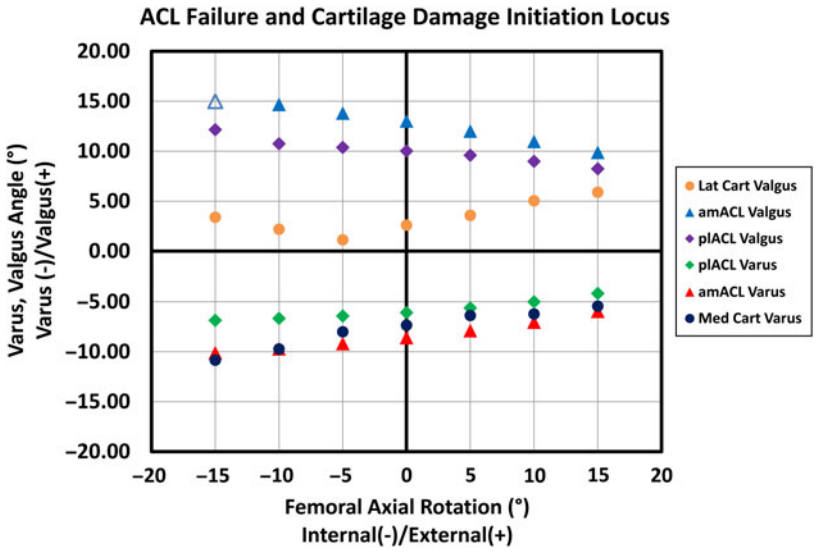

Figure 3. ACL tear initiation and tibial articular cartilage damage locus relative to the subjects initial frontal plane alignment of 7.67° valgus. The figure provides the relationship between knee orientation and knee tissue failure. The locus shows lateral tibial articular cartilage failure for valgus motions (Lat Cart Valgus), medial tibial articular cartilage failure for varus motions (Med Cart Varus), and both amACL and plACL failure for varus and valgus motions.

the tibia, or the tibia with respect to the femur. The femur was moved with respect to the tibia by fixing the tibia to the ground as this simulated closed chain foot-to-ground contact. The axis of rotation for I/E femoral rotation was the line normal to the tibial plateau intersecting the midpoint of the femoral trans-epicondylar axis. Figure 1(c) shows the boundary conditions for these simulations. Each simulation had a unique axial femoral rotation angle ranging from 15° IR to 15° ER in 5° increments (7 increments of axial rotation with varus +7 increments of axial rotation with valgus = 14 total simulations).

ACL failure locus points were processed by tracking the normal stress within the mid-substance of both ACL bundles. Each simulation produced data points indicating the frontal plane knee angle at tear initiation for both bundles. The simulations also provided tibial articular cartilage damage data. This included the frontal plane knee angle at cartilage damage initiation as well as the extent of cartilage damage at the point of ACL failure. This produced the relationship between knee orientation and tissue injury, seen in Figure 3,[3] which shows a complete failure locus for the ACL and cartilage. The locus is divided into four quadrants, valgus/IR, valgus/ER, varus/IR, and varus/ER.

3. Results

3.1 ACL bundles: plACL versus amACL

For all simulations, the plACL required less V/V angle to reach failure compared to the amACL. In the valgus/IR quadrant, the plACL required an average of 11.1° of valgus rotation to tear, while the amACL required 14.5°, meaning 26.7% less valgus angle was needed to reach plACL failure. In the valgus/ER quadrant the plACL required on average 20.4% less valgus angle than the amACL to reach failure. In the varus/IR quadrant the plACL required on average 36.8% less varus angle than the amACL to reach failure. In the varus/ER quadrant the plACL required on average 34.0% less varus angle than the amACL to reach failure. The average combined (varus and valgus) failure angle for the plACLwas 7.9°, while the average combined failure angle for the amACL was 10.6°. Overall, the plACL was 28.5% more susceptible to tearing than the amACL. Complete ACL tear occurs when both bundles rupture. The data demonstrates that complete ACL tear is more likely to occur in ER than in IR. Furthermore, the results indicate that the ACL is more prone to complete rupture in varus knee motion than in valgus motion, especially in varus/ER.

3.2 Frontal plane motion: varus versus valgus

Comparing varus motion simulations to valgus motion simulations indicated the varus motion simulations required less angle to initiate ACL tear for all degrees of I/E rotation. Comparing varus/IR to valgus/IR for the amACL, the average frontal plane knee angle at tear initiation for varus/IR was 9.7° varus, while in valgus/IR it was 14.5° valgus, a 40.1% increase in frontal plane knee angle at amACL failure from varus/IR to valgus/IR. The same comparison performed on the plACL resulted in a 50.0% increase in frontal plane knee angle at plACL failure from varus/IR to valgus/IR. Comparing varus/ER

to valgus/ER for the amACL, the average frontal plane knee angle for varus/ER was 7.0° varus, while in valgus/ER it was 11.0° valgus, indicating a 44.8% increase in the frontal plane knee angle at amACL failure from varus/ER to valgus/ER. The same comparison for plACL resulted in a 57.7% increase in frontal plane knee angle at plACL failure from varus/ER to valgus/ER. Overall, varus simulations required 46.6% less frontal plane knee angle for tear initiation compared to valgus simulations.

3.3 *Transverse plane motion: ER versus IR*

The ER simulations required less V/V angle for ACL failure compared to IR simulations. Looking at valgus simulations, the average amACL valgus failure angle in the valgus/IR quadrant was 14.5° compared to 11.0° in the valgus/ER quadrant indicating a 27.8% decrease in valgus failure angle from valgus/IR to valgus/ER. The same analysis on the plACL in valgus resulted in a 21.5% decrease from valgus/IR to valgus/ER. Looking at varus simulations, the average amACL varus tear initiation angle in varus/IR was 9.7° compared to 7.0° in varus/ER indicating a 32.5% decrease in varus failure angle from varus/IR to varus/ER. The same analysis on the plACL in varus resulted in a 29.7% decrease from varus/IR to varus/ER. Overall, ER decreased the V/V failure angle by 27.5% relative to IR.

3.4 *Articular cartilage injury*

In all valgus cases, articular cartilage injury initiation occurred prior to ACL failure, Figure 3. In varus cases, it occurred in between the amACL and plACL bundle failures in six out of the seven simulations. For valgus cases, the average injury initiation angle for articular cartilage was 3.2° valgus. For varus cases the average articular cartilage injury angle was 7.6° varus. The varus/IR simulations demonstrated greater varus angles at articular cartilage injury compared to the varus/ER simulations, following a similar trend as the ACL bundle failures. This was not seen in valgus, as an increase in both ER and IR increased the valgus injury initiation angle for the articular cartilage. In valgus simulations, the most detrimental orientation for articular cartilage injury initiation was 5° IR. In varus, the articular cartilage is most susceptible to injury initiation at higher degrees of ER.

The extent of articular cartilage damage at ACL failure was much higher in valgus cases than in varus cases. This is because articular cartilage injury initiated

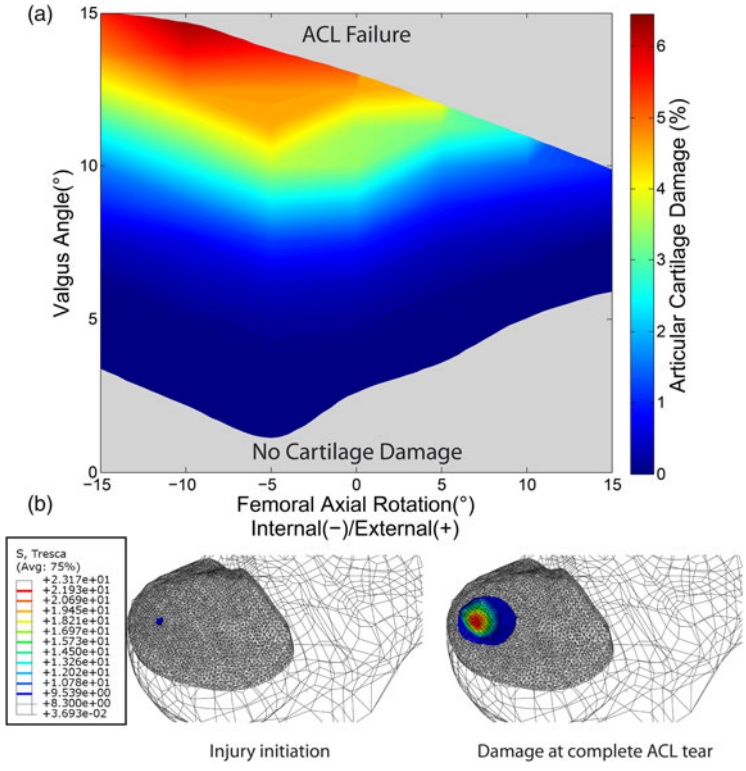

Figure 4. (a) Articular cartilage damage map reporting the % volume of damaged tissue relative to femoral axial rotation and valgus angle. (b) Isosurface plot of the 10° IR valgus simulation showing the growth in articular cartilage damage from injury initiation at $\tau_{max} = 4.15$ MPa to the time of ACL failure. Here, Tresca stress is defined as $2*\tau_{max}$.

prior to ACL failure in valgus while in varus it occurred coincidentally with ACL tear initiation. Thus, it was only necessary to investigate the extent of articular cartilage damage for the valgus cases. The results, seen in Figure 4(a), indicate that with greater IR there will be greater articular cartilage damage at ACL failure for valgus cases. This is in part due to ACL failure occurring at greater degrees of valgus when in internal rotation. If an ACL injury were to occur in IR, the cartilage damage would be greater compared to that seen from an ACL injury occurring in ER. Figure 4(b) demonstrates the growth of the lateral articular cartilage injury from initiation until ACL failure for the 10° IR valgus case. As indicated before, damage extent should be considered as an estimate as the exact constitutive equations of damaged tissue and critical stress required for damage growth are not available at this time. Regardless, the results indicate that the extent of cartilage injury is greater when ACL failure occurs in valgus motion compared to varus motion.

4. Discussion

The accuracy of the FE model used in this investigation was validated in our previous investigations (Homyk et al. 2012). The results from Homyk et al. (2012) compared well with the published experimental data reported by Rupp et al. (1999). Rupp et al. (1999) performed cadaver knee experiments, measuring patellar tendon ACL graft forces under various loading conditions. ACL graft tension was recorded due to valgus moments of 5 N · m and 15 N · m and varus moments of 5 N · m and 15 N · m at 30° and 60° of knee flexion, respectively. Using the model from this study, simulations were performed using the same loading conditions to compare results with Rupp et al. (1999). The ACL forces from the model used in this investigation compared well with the ACL forces reported by Rupp et al. (1999).

In a previous investigation, the ACL was modeled using a viscohyperelastic material to understand the effect of loading rate on ACL rupture (Orsi 2015). The results from this previous study demonstrated no difference existed in the frontal plane knee angle at ACL failure across the range of physiologically accurate loading rates (Orsi 2015). The differences between the frontal plane knee angles at ACL failure between the viscohyperelastic model and the hyperelastic model were minimal, validating the use of the time independent hyperelastic material model in this study.

In this investigation, the results obtained across all simulations indicate that the plACL was on average 28.5% more susceptible to rupture than the amACL. This may be partly due to the prestrain values at full knee extension. The plACL had 10% prestrain compared to the 6% prestrain in the amACL at full extension. The higher prestrain decreased the amount of displacement needed for tear initiation. While the plACL was more likely to tear prior to the amACL, the largest separation between the V/V failure angles for the two bundles was only 3.9°, and the average separation between bundle failures across all simulations was only 2.6°.

From the subjects' initial frontal plane alignment of 7.67° valgus, less varus angle was needed for ligament failure relative to valgus angle for all values of I/E rotation, similar to the previous study (Homyk et al. 2012). Evidence exists that supports valgus motion as the predominant injury mechanism for ACL failure (Arnold et al. 1979; Ferretti et al. 1992; Malone et al. 1993; Ireland 1999; Boden, Dean, et al. 2000; Boden, Griffin, et al. 2000). The present study indicates that varus motion may be more influential than what has been previously been understood for ACL injury. The present study does not refute the valgus mechanism theory for ACL failure; however, it is suggested that future cadaver and FE studies may be needed to confirm this finding. Based on these results, we believe that ACL injury may occur during the varus portion of the contra-coup as the knee moves from valgus to varus.

ER simulations demonstrated a 27.4% increase in ACL injury susceptibility relative to the IR simulations. This can be partially explained by the geometries of the insertion sites. With the femoral insertion located posteriorly and laterally from the tibial insertion, an applied IR will displace the femoral insertion site anteriorly and medially relative to the fixed tibial insertion. This decreases the distance between the insertion sites, decreasing ligament stress. An applied ER will do the opposite, increasing ligament stress. This increase in stress due to ER reduces the V/V failure angle for ACL injury relative to IR. Along with this, there is increased probability of a full ligament tear compared to IR simulations. Because ER increases the chance for an ACL tear by decreasing the V/V angle needed for ACL injury, and ER increases the chance of a complete tear, this suggests ER may be a more injury prone motion than IR.

The model predicted which motions will cause ACL failure and concomitant injuries. For the ACL, the valgus/ER quadrant demonstrated greater susceptibility to ACL failure than the valgus/IR quadrant. The varus/ER quadrant also demonstrated greater susceptibility to ACL failure than the varus/IR quadrant. Concomitant articular cartilage damage initiated prior to ACL failure in valgus cases, and coincidentally with the ACL in all varus simulations. Both valgus/ER and varus/ER could be argued as the most detrimental motions investigated for several reasons. First, ER had lower V/V failure angles for ACL failure. Second, in ER the articular cartilage damage initiated prior to, or in sequence with, ACL failure which increased the likelihood for concomitant injuries. Last, ER demonstrated greater susceptibility for complete ACL

rupture. The valgus/ER quadrant was arguably more detrimental compared to varus/ER as the articular cartilage damage at ACL failure is greatest.

The extent of articular cartilage damage at ACL failure was minimal in varus cases as cartilage damage initiation was coincident with ACL rupture. In valgus cases significant cartilage damage could occur prior to ACL failure. In addition, an ACL tear in valgus/IR may create the most articular cartilage damage. These results correlate well with many studies which report ER and valgus motion as leading mechanisms for ACL injury (Arnold et al. 1979; Ferretti et al. 1992; Malone et al. 1993; Ireland 1999; Boden, Dean, et al. 2000; Boden, Griffin, et al. 2000; Olsen et al. 2004; Krosshaug et al. 2007). The results also demonstrate that in addition to ACL failure occurring from this motion, cartilage injury will occur prior to ACL failure. The results are validated with available data in the literature and support the use of displacement controlled FE analyses of knee joint models to investigate subject specific tissue failure mechanisms. Other studies have used displacement controlled FE models to investigate knee joint ligament kinetics. Song et al. (2004) used a displacement controlled FE knee joint model to compare ACL forces with a cadaver experiment. They recorded the kinematics of a cadaver knee under a 134N anterior force. The cadaver model was then dissected, leaving only the two bundles of the ACL. The dissected knee was subjected to the kinematics recorded from the intact cadaver model, and the forces in the ACL bundles were recorded. An FE model of the two ACL bundles, femur, and tibia was subjected to the same kinematics, and the forces were compared with the dissected model. The FE model accurately predicted the forces in the ACL bundles (Song et al. 2004).

The present study used sequential loading analyses, while simultaneous loading simulations may better simulate *in vivo* ACL disruptions. Using sequential loading was validated as the results reported little to no difference in the V/V angle at ACL tear initiation between sequential and simultaneous loading simulations. Using sequential analysis enables independent control of I/E rotation and V/V angle, allowing the results to reveal the dominant motion causing the injury. Such an understanding is not possible using simultaneous loading. By using displacement controlled simulations, the results will determine the tibiofemoral orientations causing damage or injury to knee joint tissue. For this procedure it is not required to know muscle forces. This is beneficial as modeling the subject specific muscular forces is complex and inaccurate. Material properties for the various tissues included in our model were taken from several recent publications which have been used and validated in several simulation based studies (Blankevoort et al. 1991; Puso et al. 1998; Haut Donohue 2002; Fung and Zhang 2003; Haut Donahue et al. 2003; Peña et al. 2006; Yang et al. 2010a; Wangerin 2013; Kiapour et al. 2014). It is known that ACL injury and cartilage damage will change the material properties of these soft tissues. Accurately developing a constitutive model for damaged soft tissue is extremely complex. This requires numerous careful experimental investigations to properly establish the constitutive equations for the damaged tissue. As an accurate material model for damaged tissue has yet to be determined, the material properties did not change through our investigation. The cartilage damage initiation results should be considered reliable; however, the cartilage damage growth up until ACL injury may be underestimated. It should be noted that because the simulations are displacement controlled, the extent of articular cartilage damage will have little effect on the ACL failure results. As stated earlier, the cartilage failure criterion determined from Atkinson et al. (1998) should be viewed with discretion as this criterion was determined through *ex vivo* experimentation. Sagittal plane motion (knee flexion) was fixed at 25° in all simulations as this angle was seen as most commonly associated with ACL injury. Future investigations may be conducted to see the relationship knee flexion has on the failure locus.

This investigation highlights detrimental motions leading to ACL and concomitant injuries. The results indicate the ACL as more susceptible to injury when the knee is subjected to ER compared to IR. The results also demonstrate that cartilage injury occurred prior to ACL injury when the knee is subjected to valgus motion. The greatest amount of cartilage damage was seen during ACL injuries occurring in valgus/IR. The knee motion based tissue failure results provide valuable data for clinicians and sports medicine professionals. By better understanding how these injuries occur, orthopaedic surgeons can more accurately diagnose patients. The novel methods described in this investigation can provide individuals with their own unique ACL failure locus and may provide information that identifies individuals whom are more at risk for future ACL failure, articular cartilage pathology, and potential future osteoarthritis. Athletic training professionals can also adapt training programs to address targeted movement avoidance of injury prone motions. Physical therapy programs will benefit by incorporating strengthening for specific muscles which stabilize the knee joint against detrimental motions.

Conflict of interest disclosure statement

No potential conflict of interest was reported by the authors.

Funding

This report was made possible by a NPRP award [NPRP 5-086-2-031] from the Qatar National Research Fund (a member of The Qatar Foundation). The statements made herein are solely the responsibility of the authors.

Notes

1. Informed consent was obtained prior to MR imaging.
2. Future subject specific models can be established including higher resolution MRI with a slice thickness of 0.5 mm. Regardless of MRI resolution, this study establishes a procedure for investigating subject specific ACL failure.
3. 15° IR Valgus simulation reached ~80% amACL failure, noted by the hollow blue triangle in Figure 3.

References

Amis A, Dawkins G. 1991. British Editorial Society of Bone and Joint Surgery; Functional anatomy of the anterior cruciate ligament. Fibre bundle actions related to ligament replacements and injuries. J Bone Joint Surg. British Volume 73(2):260–267.

Arnoczky SP. 1983. LWW; Anatomy of the anterior cruciate ligament. Clin Orthop Relat Res. 172:19–25.

Arnold JA, Coker TP, Heaton LM, Park JP, Harris WD. 1979. Natural history of anterior cruciate tears. Am J Sports Med. 7(6):305–313. doi:10.1177/036354657900700601.

Askes H, de Borst R, Heeres O. 1999. Conditions for locking-free elasto-plastic analyses in the element-free Galerkin method. Comput Methods Appl Mech Eng. 173(1–2):99–109. doi:10.1016/S0045-7825(98)00259-X.

Atkinson T, Haut R, Altiero N, et al. 1998. Impact-induced fissuring of articular cartilage: an investigation of failure criteria. J Biomech Eng. 120(2):181. doi:10.1115/1.2798300.

Bell R, Houlsby G, Burd H. 1993. Suitability of three-dimensional finite elements for modelling material incompressibility using exact integration. Commun Num Methods Eng. 9(4):313–329. doi:10.1002/cnm.1640090405.

Besier TF, Lloyd DG, Cochrane JL, Ackland TR, et al. 2001. External loading of the knee joint during running and cutting maneuvers. Med Sci Sports Exerc. 33(7):1168–1175, 10.1097/00005768-200107000-00014.

Bisson LJ, Gurske-DePerio J. 2010. Axial and sagittal knee geometry as a risk factor for noncontact anterior cruciate ligament tear: a case-control study. Arthrosc J Arthrosc Relat Surg. 26(7):901–906, 10.1016/j.arthro.2009.12.012.

Blankevoort L, Kuiper J, Huiskes R, Grootenboer H. 1991. Articular contact in a three-dimensional model of the knee. J Biomech. 24(11):1019–1031. doi:10.1016/0021-9290(91)90019-J.

Boden BP, Dean GS, Feagin J, Garrett W. 2000. Slack; Mechanisms of anterior cruciate ligament injury. Orthopedics. 23(6):573–578.

Boden BP, Griffin LY, Garrett W. 2000. Etiology and prevention of noncontact ACL injury. Physician Sportsmed. 28(4):53–60. doi:10.3810/psm.2000.04.841.

Boyd J, Zavatsky A, Gill H. 2012. British Editorial Society of Bone and Joint Surgery; Subject-specific loading in the knee during functional activity: a consistent combined imaging, motion analysis and finite element approach. J Bone Joint Surg. British Volume 94(Suppl XVIII):36–36.

Butler DL, Kay MD, Stouffer DC. 1986. Comparison of material properties in fascicle-bone units from human patellar tendon and knee ligaments. J Biomech. 19(6):425–432. doi:10.1016/0021-9290(86)90019-9.

Butler D, Noyes F, Grood E. 1980. Ligamentous restraints to anterior–posterior drawer in the human knee. J Bone Joint Surg Am. 62(2):259–270.

Churchill DL, Incavo SJ, Johnson CC, Beynnon BD. 1998. The transepicondylar axis approximates the optimal flexion axis of the knee. Clin Orthop Relat Res. 356:111–118. doi:10.1097/00003086-199811000-00016.

Faber KJ, Dill JR, Amendola A, Thain L, Spouge A, Fowler PJ. 1999. American Orthopaedic Society for Sports Medicine; Occult osteochondral lesions after anterior cruciate ligament rupture six-year magnetic resonance imaging follow-up study. Am J Sports Med. 27(4):489–494.

Feagin, Jr, J, Lambert K. 1985. Mechanism of injury and pathology of anterior cruciate ligament injuries. Orthop Clin North Am. 16(1):41–45.

Ferretti A, Papandrea P, Conteduca F, Mariani PP. 1992. Knee ligament injuries in volleyball players. Am J Sports Med. 20(2):203–207. doi:10.1177/036354659202000219.

Fleming BC, Oksendahl HL, Mehan WA, Portnoy R, Fadale PD, Hulstyn MJ, Bowers ME, Machan JT, Tung GA. 2010. Delayed gadolinium-enhanced MR imaging of cartilage (dGEMRIC) following ACL injury. Osteoarthritis Cartilage. 18(5):662–667. doi:10.1016/j.joca.2010.01.009.

Fukubayashi T, Torzilli P, Sherman M, Warren R. 1982. The Journal of Bone and Joint Surgery, Inc.; An *in vitro* biomechanical evaluation of anterior–posterior motion of the knee. Tibial displacement, rotation, and torque. J Bone Joint Surg. 64(2):258–264.

Fung DT, Zhang LQ. 2003. Modeling of ACL impingement against the intercondylar notch. Clin Biomech. 18(10):933–941. doi:10.1016/S0268-0033(03)00174-8.

Gardiner JC, Weiss JA. 2003. Subject-specific finite element analysis of the human medial collateral ligament during valgus knee loading. J Orthop Res. 21(6):1098–1106. doi:10.1016/S0736-0266(03)00113-X.

Girgis FG, Marshall JL, Jem AAM. 1975. The cruciate ligaments of the knee joint: anatomical. Functional and Experimental Analysis. Clin Orthop Relat Res. 106:216–231. doi:10.1097/00003086-197501000-00033.

Griffin LY, Albohm MJ, Arendt EA, Bahr R, Beynnon BD, DeMaio M, Dick RW, Engebretsen L, Garrett WE, Hannafin JA, et al. 2006. Understanding and preventing noncontact anterior cruciate ligament injuries: a review of the hunt valley II meeting, January 2005. Am J Sports Med. 34(9):1512–1532. doi:10.1177/0363546506286866.

Grood E, Noyes F, Butler D, Suntay W. 1981. Ligamentous and capsular restraints preventing straight medial and lateral laxity in intact human cadaver knees. J Bone Joint Surg Am. 63:1257–1269.

Gründer W, Kanowski M, Wagner M, Werner A. 2000. Wiley Online Library; Visualization of pressure distribution within loaded joint cartilage by application of angle-sensitive NMR microscopy. Magn Reson Med. 43(6): 884–891.

Hashemi J, Chandrashekar N, Mansouri H, Gill B, Slauterbeck JR, Schutt RC, Dabezies E, Beynnon BD. 2010. Shallow medial tibial plateau and steep medial and lateral tibial slopes: new risk factors for anterior cruciate ligament injuries. Am J Sports Med. 38(1):54–62. doi:10.1177/0363546509349055.

Haut Donahue T, Hull M, Rashid MM, Jacobs CR. 2003. How the stiffness of meniscal attachments and meniscal material properties affect tibio-femoral contact pressure computed using a validated finite element model of the human knee joint. J Biomech. 36(1):19–34. doi:10.1016/S0021-9290(02)00305-6.

Herberhold C, Faber S, Stammberger T, Steinlechner M, Putz R, Englmeier K, Reiser M, Eckstein F. 1999. *In situ* measurement of articular cartilage deformation in intact

femoropatellar joints under static loading. J Biomech. 32(12):1287–1295. doi:10.1016/S0021-9290(99)00130-X.

Hollister AM, Jatana S, Singh AK, Sullivan WW, Lupichuk AG. 1993. LWW; The axes of rotation of the knee. Clin Orthop Relat Res. 290:259–268.

Homyk A, Orsi A, Wibby S, Yang N, Nayeb-Hashemi H, Canavan PK. 2012. Failure locus of the anterior cruciate ligament: 3D finite element analysis. Comput Methods Biomech Biomed Eng. 15(8):865–874. doi:10.1080/10255842.2011.565412.

Haut Donahue TL, Hull ML, Rashid MM, Jacobs CR. 2002. A finite element model of the human knee joint for the study of tibio-femoral contact. J Biomech Eng. 124(3):273–280. doi:10.1115/1.1470171.

Ireland ML. 1999. National Athletic Trainers Association; Anterior cruciate ligament injury in female athletes: epidemiology. J Athlet Train. 34(2):150–154.

Johnson DL, Urban WP, Caborn DN, Vanarthos WJ, Carlson CS. 1998. American Orthopaedic Society for Sports Medicine; Articular cartilage changes seen with magnetic resonance imaging-detected bone bruises associated with acute anterior cruciate ligament rupture. Am J sports Med. 26(3):409–414.

Kennedy J, Hawkins R, Willis R, Danylchuk K. 1976. Tension studies of human knee ligaments. J Bone Joint Surg Am. 58:350–355.

Kiapour A, Kiapour AM, Kaul V, Quatman CE, Wordeman SC, Hewett TE, Demetropoulos CK, Goel VK. 2014. Finite element model of the knee for investigation of injury mechanisms: development and validation. J Biomech Eng. 136(1):011002. doi:10.1115/1.4025692.

Krosshaug T, Nakamae A, Boden BP, Engebretsen L, Smith G, Slauterbeck JR, Hewett TE, Bahr R. 2007. Mechanisms of anterior cruciate ligament injury in basketball: video analysis of 39 cases. Am J Sports Med. 35(3):359–367. doi:10.1177/0363546506293899.

Limbert. 2004. Three-dimensional finite element modelling of the human ACL: simulation of passive knee flexion with a stressed and stress-free ACL. J Biomech. 37(11):1723–1731. doi:10.1016/j.jbiomech.2004.01.030.

Malone T, Hardaker W, Garrett W, Feagin J, Bassett F. 1993. Relationship of gender to anterior cruciate ligament injuries in intercollegiate basketball players. J South Orthop Assoc. 2(1):36–39.

Markolf KL, Mensch J, Amstutz H. 1976. The Journal of Bone and Joint Surgery, Inc.; Stiffness and laxity of the knee – the contributions of the supporting structures. A quantitative *in vitro* study. J Bone Joint Surg. 58(5):583–594.

McNair P, Marshall R, Matheson J, et al. 1990. Important features associated with acute anterior cruciate ligament injury. N Z Med J. 103(901):537–539.

Mesfar W, Shirazi-Adl A. 2006. Biomechanics of changes in ACL and PCL material properties or prestrains in flexion under muscle force-implications in ligament reconstruction. Comput Methods Biomech Biomed Eng. 9(4):201–209. doi:10.1080/10255840600795959.

Nau T, Teuschl A. 2015. Regeneration of the anterior cruciate ligament: current strategies in tissue engineering. World J Orthop. 6(1):127. doi:10.5312/wjo.v6.i1.127.

Nishii T, Kuroda K, Matsuoka Y, Sahara T, Yoshikawa H. 2008. Change in knee cartilage T2 in response to mechanical loading. J Magn Reson Imaging. 28(1):175–180. doi:10.1002/jmri.21418.

Noyes FR, Grood ES, et al. 1976. The strength of the anterior cruciate ligament in humans and Rhesus monkeys. J Bone Joint Surg. American Volume 58(8):1074–1082.

Olsen OE, Myklebust G, Engebretsen L, Bahr R. 2004. Injury mechanisms for anterior cruciate ligament injuries in team handball: a systematic video analysis. Am J Sports Med. 32(4):1002–1012. doi:10.1177/0363546503261724.

Orsi AD. 2015. Bioengineering Department, Northeastern University; New approaches in finite element modeling for understanding knee joint injuries [Thesis], Under preparation.

Papaioannou G, Demetropoulos CK, King YH. 2010. Predicting the effects of knee focal articular surface injury with a patient-specific finite element model. Knee. 17(1):61–68. doi:10.1016/j.knee.2009.05.001.

Papaioannou G, Nianios G, Mitrogiannis C, Fyhrie D, Tashman S, Yang K. 2008. Patient-specific knee joint finite element model validation with high-accuracy kinematics from biplane dynamic roentgen stereogrammetric analysis. J Biomech. 41(12):2633–2638. doi:10.1016/j.jbiomech.2008.06.027.

Park HS, Ahn C, Fung DT, Ren Y, Zhang LQ. 2010. A knee-specific finite element analysis of the human anterior cruciate ligament impingement against the femoral intercondylar notch. J Biomech. 43(10):2039–2042. doi:10.1016/j.jbiomech.2010.03.015.

Peña E, Calvo B, Martinez M, Doblare M. 2006. Elsevier; A three-dimensional finite element analysis of the combined behavior of ligaments and menisci in the healthy human knee joint. J Biomech. 39(9):1686–1701.

Puso M, Weiss J, et al. 1998. Finite element implementation of anisotropic quasi-linear viscoelasticity using a discrete spectrum approximation. J Biomech Eng. 120(1):62. doi:10.1115/1.2834308.

Renstrom PP, Ljungqvist AA, Arendt EE, Beynnon BB, Fukubayashi TT, Garrett WW, Georgoulis TT, Hewett T ETE, Johnson RR, Krosshaug TT, et al. 2008. Non-contact ACL injuries in female athletes: an international Olympic Committee current concepts statement. Br J Sports Med. 42(6):394–412. doi:10.1136/bjsm.2008.048934.

Rupp S, Hopf T, Hess T, Seil R, Kohn DM. 1999. Resulting tensile forces in the human bone – patellar tendon – bone graft: direct force measurement *in vitro*. Arthrosc J Arthrosc Relat Surg. 15(2):179–184. doi:10.1053/ar.1999.v15.0150171.

Simon R, Everhart J, Nagaraja H, Chaudhari A. 2010. A case-control study of anterior cruciate ligament volume, tibial plateau slopes and intercondylar notch dimensions in ACL-injured knees. J Biomech. 43(9):1702–1707. doi:10.1016/j.jbiomech.2010.02.033.

Sinkov VA, Andres BM, Wheeless CR, Frassica FJ. 2004. Internet-based learning. Clin Orthop Relat Res. 421:99–106. doi:10.1097/01.blo.0000126944.23557.5c.

Smith HC, Johnson RJ, Shultz SJ, Tourville T, Holterman LA, Slauterbeck J, Vacek PM, Beynnon BD. 2012. A prospective evaluation of the landing error scoring system (LESS) as a screening tool for anterior cruciate ligament injury risk. Am J Sports Med. 40(3):521–526. doi:10.1177/0363546511429776.

Song Y, Debski RE, Musahl V, Thomas M, Woo SLY. 2004. A three-dimensional finite element model of the human anterior cruciate ligament: a computational analysis with experimental validation. J Biomech. 37(3):383–390. doi:10.1016/S0021-9290(03)00261-6.

Steckel H, Starman J, Baums M, Klinger H, Schultz W, Fu F. 2007. Wiley Online Library; Anatomy of the anterior cruciate ligament double bundle structure: a macroscopic evaluation. Scand J Med Sci Sports. 17(4):387–392.

Takahashi M, Doi M, Abe M, Suzuki D, Nagano A. 2006. Anatomical study of the femoral and tibial insertions of the anteromedial and posterolateral bundles of human anterior cruciate ligament. Am J Sports Med. 34(5):787–792. doi:10.1177/0363546505282625.

Vedi V, Williams E, Tennant A, Spouse S, Hunt D, Gedroyc W. 1999. Meniscal movement An in-vivo study using dynamic MRI. J Bone Joint Surg. 81(1):37–41. doi:10.1302/0301-620X.81B1.8928.

Vellet AD, Marks P, Fowler P, Munro T. 1991. Occult posttraumatic osteochondral lesions of the knee: prevalence, classification, and short-term sequelae evaluated with MR imaging. Radiology. 178(1):271–276. doi:10.1148/radiology.178.1.1984319.

Wang Y, Fan Y, Zhang M. 2014. Comparison of stress on knee cartilage during kneeling and standing using finite element models. Med Eng Phys. 36(4):439–447. doi:10.1016/j.medengphy.2014.01.004.

Wangerin S. 2013. Development and validation of a human knee joint finite element model for tissue stress and strain predictions during exercise. San Luis Obispo: California Polytechnic State University.

Woo SLY, Hollis JM, Adams DJ, Lyon RM, Takai S, et al. 1991. Tensile properties of the human femur-anterior cruciate ligament-tibia complex: the effects of specimen age and orientation. Am J Sports Med. 19(3):217–225. doi:10.1177/036354659101900303.

Yang NH, Nayeb-Hashemi H, Canavan PK. 2009. The combined effect of frontal plane tibiofemoral knee angle and meniscectomy on the cartilage contact stresses and strains. Annals Biomed Eng. 37(11):2360–2372.

Yang NH, Canavan PK, Nayeb-Hashemi H. 2010a. The effect of the frontal plane tibiofemoral angle and varus knee moment on the contact stress and strain at the knee cartilage. J Appl Biomech. 26(4):432–443.

Yang NH, Canavan PK, Nayeb-Hashemi H, Najafi B, Vaziri A. 2010b. Protocol for constructing subject-specific biomechanical models of knee joint. Comput methods Biomech Biomed Eng. 13(5):589–603.